

**Possible strategy of discriminating 1D new physics solutions in  $b \rightarrow s\ell\ell$  decays after  
Moriond 2021**

Shuang-Yi Li,<sup>1</sup> Rui-Xiang Shi,<sup>1</sup> and Li-Sheng Geng<sup>2,3,\*</sup>

<sup>1</sup>*School of Physics, Beihang University, Beijing 102206, China*

<sup>2</sup>*School of Physics & Beijing Key Laboratory of Advanced Nuclear Materials and Physics,  
Beihang University, Beijing 102206, China*

<sup>3</sup>*School of Physics and Microelectronics,  
Zhengzhou University, Zhengzhou, Henan 450001, China*

**Abstract**

The recent measurements of  $R_K, B_s \rightarrow \mu^+\mu^-$ , a set of CP-averaged angular observables for the  $B^0 \rightarrow K^{*0}\mu^+\mu^-$  decay, and its isospin partner  $B^+ \rightarrow K^{*+}\mu^+\mu^-$  by the LHCb Collaboration, consistently hint at lepton universality violation in the  $b \rightarrow s\ell\ell$  transitions. The so-called  $B$  anomalies can be best explained in five one-dimensional scenarios, i.e.,  $\delta C_9^\mu, \delta C_{10}^\mu, \delta C_L^\mu, \delta C_9^\mu = C_{10}^{\mu'}$ , and  $\delta C_9^\mu = -C_9^{\mu'}$ . In this work we explore how these scenarios can be distinguished from each other. We first study the combinations of four angular asymmetries  $A_i$  ( $i = 3, 4, 5, 9$ ) and find that they cannot distinguish the five new physics scenarios. We then show that the two ratios  $R_{1s}$  and  $R_{2s}$  can uniquely discriminate the five new physics scenarios in proper intervals of  $q^2$  if they can be measured with a percent level precision.

---

\* E-mail:lisheng.geng@buaa.edu.cn

## I. INTRODUCTION

In the standard model (SM), the rare decays of  $B$  mesons induced by flavour-changing neutral-current (FCNC)  $b \rightarrow s\ell\ell$  transition at the quark level are suppressed by the GIM mechanism [1]. Therefore they provide an ideal laboratory to indirectly probe new physics (NP) beyond the SM. Interestingly, the measurements of several observables yield results in tension with the SM expectations (see Refs. [2, 3] for recent reviews).

Recently, the LHCb Collaboration reported the most precise measurement of  $R_K = \Gamma(B \rightarrow K\mu\mu)/\Gamma(B \rightarrow Kee)$  in the bin [1.1, 6] GeV<sup>2</sup> [4]

$$R_K = 0.846_{-0.039-0.012}^{+0.042+0.013}, \quad (1)$$

showing that the significance of deviation from the SM prediction is at  $3.1\sigma$  confidence level. Compared to the 2014 measurement [5], the tension with respect to the SM prediction has significantly increased. At the same time, a new result for the  $B_s \rightarrow \mu^+\mu^-$  branching fraction,

$$\text{BR}(B_s^0 \rightarrow \mu^+\mu^-) = (3.09_{-0.43-0.11}^{+0.46+0.15}) \times 10^{-9}, \quad (2)$$

is also published by the LHCb Collaboration [6, 7]. In Ref. [8], together with the theoretical prediction of Ref. [9] including the double-logarithmic QED and QCD corrections, the CMS measurement [10], and the ATLAS measurement [11], the following ratio is obtained

$$R = \frac{\text{BR}(B_s^0 \rightarrow \mu^+\mu^-)_{\text{exp}}}{\text{BR}(B_s^0 \rightarrow \mu^+\mu^-)_{\text{SM}}} = 0.78(9). \quad (3)$$

For the ease of comparing experimental measurements with theoretical predictions, we collect all the relevant results in Table I. In 2020, the LHCb Collaboration reported angular analyses of the  $B^0 \rightarrow K^{*0}\mu^+\mu^-$

TABLE I. Experimental data and SM predictions for the binned observables  $R_K$  and  $R_{K^*}$ . The theoretical uncertainties are estimated using the approach described in Refs. [12–14].

Observables	LHCb [4, 15]	Belle [16, 17]	SM
$R_K$ [1, 6] GeV <sup>2</sup>	–	$1.03_{-0.24}^{+0.28} \pm 0.01$	$1.0004_{-0.0007}^{+0.0008}$
$R_K$ [1.1, 6] GeV <sup>2</sup>	$0.846_{-0.039-0.012}^{+0.042+0.013}$	–	$1.0004_{-0.0007}^{+0.0008}$
$R_{K^*}$ [0.045, 1.1] GeV <sup>2</sup>	$0.66_{-0.07}^{+0.11} \pm 0.03$	$0.52_{-0.26}^{+0.36} \pm 0.06$	$0.920_{-0.006}^{+0.007}$
$R_{K^*}$ [1.1, 6] GeV <sup>2</sup>	$0.69_{-0.07}^{+0.11} \pm 0.05$	$0.96_{-0.29}^{+0.45} \pm 0.11$	$0.996_{-0.002}^{+0.002}$
$R_{K^*}$ [15, 19] GeV <sup>2</sup>	–	$1.18_{-0.32}^{+0.52} \pm 0.11$	$0.998_{-0.001}^{+0.001}$

decay and its isospin partner  $B^+ \rightarrow K^{*+}\mu^+\mu^-$  decay [18, 19]. The results reconfirm the global tension with respect to the SM predictions previously reported for the decay of  $B^0 \rightarrow K^{*0}\mu^+\mu^-$  [20].

These new measurements have attracted much attention and led to many model-independent global analyses [8, 21–28] assuming the presence of NP only in the  $b \rightarrow s\mu^+\mu^-$  mode, and it is shown that the significance of the SM exclusion in the global fits is about  $4 \sim 6\sigma$ . These data have also been explained in NP models involving tree-level exchanges of new particles such as the neutral gauge boson  $Z'$  [29, 30], leptoquarks [22, 23, 27, 31–34] or scalar Higgs [35]. It is interesting to note that the leptoquark models can simultaneously explain the  $b \rightarrow s\ell^+\ell^-$  (with  $\ell = e, \mu$ ) and charged current (CC)  $b \rightarrow c\ell^-\bar{\nu}_\ell$  (with  $\ell = \mu, \tau$ ) flavor anomalies [22, 23, 27, 33, 36].

The so-called  $B$  anomalies can be best explained in five one-dimensional scenarios, i.e.  $\delta C_9^\mu, \delta C_{10}^\mu, \delta C_L^\mu, \delta C_9^\mu = C_{10}^{\mu'}$ , and  $\delta C_9^\mu = -C_9^{\mu'}$ , as demonstrated in the model independent analyses [8, 21–25, 27, 28, 37–48]. In this work, assuming that NP appears in the muon mode <sup>1</sup>, we first present a global analysis to the  $b \rightarrow s\ell^+\ell^-$  data for two one-dimensional NP scenarios  $\delta C_9^\mu = C_{10}^{\mu'}$  and  $\delta C_9^\mu = -C_9^{\mu'}$ , which were not considered in Ref. [8]. Next, we study the four angular asymmetries  $A_i$  ( $i = 3, 4, 5, 9$ ) and find that they cannot discriminate the five new physics scenarios. Finally, we show that a set of ratios  $R_i$  are helpful to uniquely discriminate the NP scenarios. In addition, we present predictions in the SM and different NP scenarios for binned observables  $A_i$  and  $R_i$  in certain ranges of bins, which might be relevant for future experiments.

This work is organized as follows. We introduce the observables  $A_i$  and  $R_i$  in Sec. II. Results and discussions are given in Sec. III, followed by a short summary and outlook in Sec. IV.

## II. ANGULAR OBSERVABLES $A_i$ AND $R_i$ FOR THE $B \rightarrow K^*\ell^+\ell^-$ DECAY

For details about our theoretical framework, the low-energy effective Hamiltonian, the origin of theoretical uncertainties and how they are parameterized, and the statistical methods used to perform global fits of all the relevant experimental data, we refer to Ref. [8]. In this section, we introduce some angular observables which can potentially discriminate different NP scenarios. For this, we focus on the  $B \rightarrow K^*\ell^+\ell^-$  decay. The differential decay rate for the four-body  $B(p) \rightarrow K^*(k)(\rightarrow K\pi)\ell^+(q_1)\ell^-(q_2)$  decay is of the following form [12, 49]

$$\frac{d^{(4)}\Gamma}{dq^2 d \cos \theta_\ell d \cos \theta_K d\phi} = \frac{9}{32\pi} I^{(\ell)}(q^2, \theta_\ell, \theta_K, \phi), \quad (4)$$

<sup>1</sup> For a discussion about the scenario where NP appears in both the electron and muon channels, see Appendix A.

with

$$\begin{aligned}
I^{(\ell)}(q^2, \theta_\ell, \theta_K, \phi) = & (I_1^s \sin^2 \theta_K + I_1^c \cos^2 \theta_K + (I_2^s \sin^2 \theta_K + I_2^c \cos^2 \theta_K) \cos 2\theta_\ell \\
& + I_3 \sin^2 \theta_K \sin^2 \theta_\ell \cos 2\phi + I_4 \sin 2\theta_K \sin 2\theta_\ell \cos \phi \\
& + I_5 \sin 2\theta_K \sin \theta_\ell \cos \phi \\
& + (I_6^s \sin^2 \theta_K + I_6^c \cos^2 \theta_K) \cos \theta_\ell + I_7 \sin 2\theta_K \sin \theta_\ell \sin \phi \\
& + I_8 \sin 2\theta_K \sin 2\theta_\ell \sin \phi + I_9 \sin^2 \theta_K \sin^2 \theta_\ell \sin 2\phi), \tag{5}
\end{aligned}$$

where the kinematics variables  $q^2$ ,  $\theta_\ell$ ,  $\theta_K$  and  $\phi$  are defined, respectively, as follows: (i)  $q^2 = (p - k)^2$  is the square of the dilepton invariant mass, (ii)  $\theta_\ell$  is the angle between the flight direction of the  $B$  meson and the  $\ell^-$  lepton in the dilepton rest frame, (iii)  $\theta_K$  is the angle between momenta of the  $B$  meson and the  $K$  meson in the dimeson ( $K\pi$ ) rest frame, (iv)  $\phi$  is the angle between the dimeson ( $K\pi$ ) and dilepton rest frames. As shown in Fig. 1, both  $\theta_\ell$  and  $\theta_K$  are defined in the interval  $[0, \pi]$  while the range of  $\phi$  is  $[0, 2\pi]$ . The angular coefficients  $I_i$  expressed in terms of the helicity amplitudes can be found in Ref. [12], while the expressions of the CP-conjugate decay  $\bar{B} \rightarrow \bar{K}^* \ell^+ \ell^-$  can be obtained by the following replacements

$$I_{1s(c),2s(c),3,4,7} \rightarrow \bar{I}_{1s(c),2s(c),3,4,7}, \quad I_{5,6,8,9} \rightarrow -\bar{I}_{5,6,8,9}, \tag{6}$$

where  $\bar{I}_i = I_i^*$ .

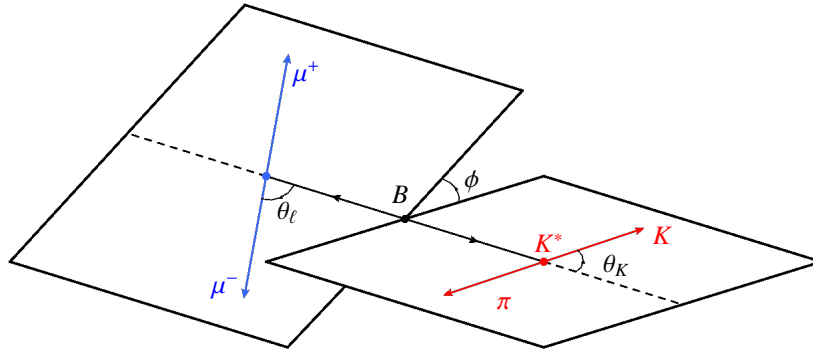


FIG. 1. Kinematics of the  $B \rightarrow K^* \ell^+ \ell^-$  decay.

Following the strategy outlined in Refs. [50, 51], we can “construct” four angular asymmetries  $A_i$  ( $i = 3, 4, 5, 9$ ) by integrating over different intervals in the angles  $\theta_\ell$ ,  $\theta_K$ , and  $\phi$  for the  $B \rightarrow K^* \mu^+ \mu^-$  decay as

follows:

$$\begin{aligned}
A_3(q^2) &= \frac{\left[ \int_{-\pi/4}^{\pi/4} - \int_{\pi/4}^{3\pi/4} + \int_{-3\pi/4}^{3\pi/4} - \int_{3\pi/4}^{7\pi/4} \right] d\phi \int_{-1}^1 d \cos \theta_K \int_{-1}^1 d \cos \theta_\ell \cdot I_{\text{sum}}(q^2, \theta_\ell, \theta_K, \phi)}{\int_0^{2\pi} d\phi \int_{-1}^1 d \cos \theta_K \int_{-1}^1 d \cos \theta_\ell \cdot I_{\text{sum}}(q^2, \theta_\ell, \theta_K, \phi)}, \\
A_4(q^2) &= \frac{\left[ \int_0^{\pi/2} - \int_{\pi/2}^\pi + \int_0^\pi - \int_\pi^{2\pi} \right] d\phi \left[ \int_0^1 - \int_{-1}^0 \right] d \cos \theta_K \left[ \int_0^1 - \int_{-1}^0 \right] d \cos \theta_\ell \cdot I_{\text{sum}}(q^2, \theta_\ell, \theta_K, \phi)}{\int_0^{2\pi} d\phi \int_{-1}^1 d \cos \theta_K \int_{-1}^1 d \cos \theta_\ell \cdot I_{\text{sum}}(q^2, \theta_\ell, \theta_K, \phi)}, \\
A_5(q^2) &= \frac{\left[ \int_0^{\pi/2} - \int_{\pi/2}^\pi + \int_0^\pi - \int_\pi^{2\pi} \right] d\phi \left[ \int_0^1 - \int_{-1}^0 \right] d \cos \theta_K \int_{-1}^1 d \cos \theta_\ell \cdot I_{\text{diff}}(q^2, \theta_\ell, \theta_K, \phi)}{\int_0^{2\pi} d\phi \int_{-1}^1 d \cos \theta_K \int_{-1}^1 d \cos \theta_\ell \cdot I_{\text{sum}}(q^2, \theta_\ell, \theta_K, \phi)}, \\
A_9(q^2) &= \frac{\left[ \int_0^{\pi/2} - \int_{\pi/2}^\pi + \int_0^\pi - \int_\pi^{2\pi} \right] d\phi \int_{-1}^1 d \cos \theta_K \int_{-1}^1 d \cos \theta_\ell \cdot I_{\text{diff}}(q^2, \theta_\ell, \theta_K, \phi)}{\int_0^{2\pi} d\phi \int_{-1}^1 d \cos \theta_K \int_{-1}^1 d \cos \theta_\ell \cdot I_{\text{sum}}(q^2, \theta_\ell, \theta_K, \phi)}, \tag{7}
\end{aligned}$$

with

$$\begin{aligned}
I_{\text{sum}}(q^2, \theta_\ell, \theta_K, \phi) &= I^{(\ell)}(q^2, \theta_\ell, \theta_K, \phi) + \bar{I}^{(\ell)}(q^2, \theta_\ell, \theta_K, \phi), \\
I_{\text{diff}}(q^2, \theta_\ell, \theta_K, \phi) &= I^{(\ell)}(q^2, \theta_\ell, \theta_K, \phi) - \bar{I}^{(\ell)}(q^2, \theta_\ell, \theta_K, \phi), \tag{8}
\end{aligned}$$

where the angular asymmetries  $A_i$  are related to the CP-averaged observables  $S_i$ ,<sup>2</sup> namely,

$$\begin{aligned}
A_3 &= \frac{1}{\pi} S_3, & A_4 &= \frac{1}{\pi} S_4, \\
A_5 &= \frac{3}{8} S_5, & A_9 &= \frac{1}{\pi} S_9. \tag{10}
\end{aligned}$$

Clearly, analogous to  $S_i$  [49, 52, 53], the observables  $A_i$  are also sensitive to NP. As a matter of fact, the relative uncertainties of observables  $A_i$  and those of  $S_i$  are equal. On the experimental side, these observables can be measured either by fitting to angular distributions, or by performing angular integrations of  $I_i$ . However, this may result in different statistical uncertainties because of different angular coverages. It should be noted that the observables  $A_i$  are ratios of combinations of the well-known angular coefficients  $I_i$ . Therefore it is feasible to measure them in the current experiments and their uncertainties are under control.

In addition to the  $A_i$  observables, following Refs. [13, 14], we revisit the angular observables  $R_i$ ,

$$R_i(q^2) = \frac{I_i^{(\mu)}(q^2) + \bar{I}_i^{(\mu)}(q^2)}{I_i^{(e)}(q^2) + \bar{I}_i^{(e)}(q^2)}, \tag{11}$$

which are defined with different angular coefficients in Eq. (5). As pointed out in Ref. [13], the observables  $R_i$  are sensitive to new physics and their hadronic uncertainties are almost exactly cancelled in the ratios. It should be emphasized that in this work the lepton mass  $m_\ell$  is non-vanishing and the angular coefficient  $I_0^C$  is absent because we donot consider scalar operators.

<sup>2</sup> The CP-averaged observables are introduced in Ref. [49] as

$$S_i(q^2) = \frac{I_i(q^2) + \bar{I}_i(q^2)}{d(\Gamma + \bar{\Gamma})/dq^2}. \tag{9}$$

### III. RESULTS AND DISCUSSIONS

In this section, we first present two more global fits using the new data from Refs. [4, 10, 11, 16–19, 54], in comparison with Ref. [8]. Next, we study whether with the four asymmetry observables  $A_i$  and the ratios  $R_i$  constructed in Refs. [13, 14], one can distinguish different one-dimensional NP scenarios.

In our recent work [8], it is shown that the three one-dimensional scenarios  $\delta C_9^\mu$ ,  $\delta C_{10}^\mu$  and  $\delta C_L^\mu = \delta C_9^\mu = -\delta C_{10}^\mu$  can well describe the current experimental data. In fact, in the case of NP involving tree-level exchanges of new particles such as the neutral gauge boson  $Z'$ , leptoquarks or scalar Higgs, further correlations can be induced between the Wilson coefficients  $C_9^{\mu(r)}$  and  $C_{10}^{\mu(r)}$ . As demonstrated in some model independent analyses [24, 37, 40–42, 45, 48], two additional one-dimensional scenarios  $\delta C_9^\mu = C_{10}^{\mu'}$  and  $\delta C_9^\mu = -C_9^{\mu'}$  cannot be completely excluded by the current  $b \rightarrow s\ell\ell$  data. The former scenario can be realized in the  $U_1$  leptoquark model in the case of  $\mathbf{g}_{\ell q}^{\mu b} (\mathbf{g}_{\ell q}^{\mu s})^* = \mathbf{g}_{ed}^{\mu b} (\mathbf{g}_{ed}^{\mu s})^*$  [33]. The latter one could be realized in  $Z'$  models with vector-like fermions and  $L_\mu - L_\tau$  symmetry [55]. Therefore, we would like to investigate these two NP scenarios in our theoretical framework. This can be done following the same strategy as that of Ref. [8] and the corresponding results are shown in Table II. We note that the  $\delta C_9^\mu = C_{10}^{\mu'}$  and  $\delta C_9^\mu = -C_9^{\mu'}$  scenarios can well explain the new  $b \rightarrow s\ell\ell$  data and the deviation from the SM has a significance of more than  $3\sigma$ , smaller than the three one-dimensional scenarios studied in Ref. [8]. Indeed, we also tested the other one-dimensional scenarios induced by NP models with the new data studied in the present work and found that they are excluded at  $3\sigma$  confidence level, consistent with the conclusions of Refs. [24, 37, 40–42, 45, 48].

TABLE II. Best fit values,  $\chi_{\min}^2$ ,  $p$ -value,  $\text{Pull}_{\text{SM}}$  and confidence intervals of the WCs in the five one dimensional scenarios. The results of  $\delta C_9^\mu$ ,  $\delta C_{10}^\mu$  and  $\delta C_L^\mu$  [8] are also shown for comparison.

Coeff.	best fit	$\chi_{\min}^2$	$p$ -value	$\text{Pull}_{\text{SM}}$	$1\sigma$ range	$3\sigma$ range
$\delta C_9^\mu = C_{10}^{\mu'}$	-0.45	115.39 [93 dof]	0.06	3.39	[-0.59, -0.32]	[-0.85, -0.05]
$\delta C_9^\mu = -C_9^{\mu'}$	-1.00	114.85 [93 dof]	0.06	3.47	[-1.29, -0.71]	[-1.90, -0.14]
$\delta C_9^\mu$ [8]	-0.85	106.32 [93 dof]	0.16	4.53	[-1.06, -0.64]	[-1.50, -0.27]
$\delta C_{10}^\mu$ [8]	0.54	107.82 [93 dof]	0.14	4.37	[0.41, 0.67]	[0.16, 0.94]
$\delta C_L^\mu$ [8]	-0.39	102.81 [93 dof]	0.23	4.91	[-0.48, -0.31]	[-0.65, -0.15]

As discussed above, among the new NP scenarios studied, all of the five one-dimensional cases, i.e.,  $\delta C_9^\mu$ ,  $\delta C_{10}^\mu$ ,  $\delta C_L^\mu$ ,  $\delta C_9^\mu = C_{10}^{\mu'}$  and  $\delta C_9^\mu = -C_9^{\mu'}$ , can provide a good description of the latest data. Thus, a natural question is which observables can discriminate between them. For such a purpose, we study the four angular asymmetries  $A_i$  ( $i = 3, 4, 5, 9$ ) and the set of ratios  $R_i$  introduced in Sec. II.

### A. Sensitivity of angular asymmetries $A_i$ to new physics

In Fig. 2, we plot  $A_{3,5,4,9}$  as functions of  $q^2$ , where  $q$  is the dilepton invariant mass, with the best fitted Wilson coefficients determined for the SM and the five one-dimensional NP scenarios. The shaded bands reflect the uncertainties originating from form factors and contributions of charm loops [12–14]. The asymmetries integrated over [15,19] GeV<sup>2</sup> are given in Table III.

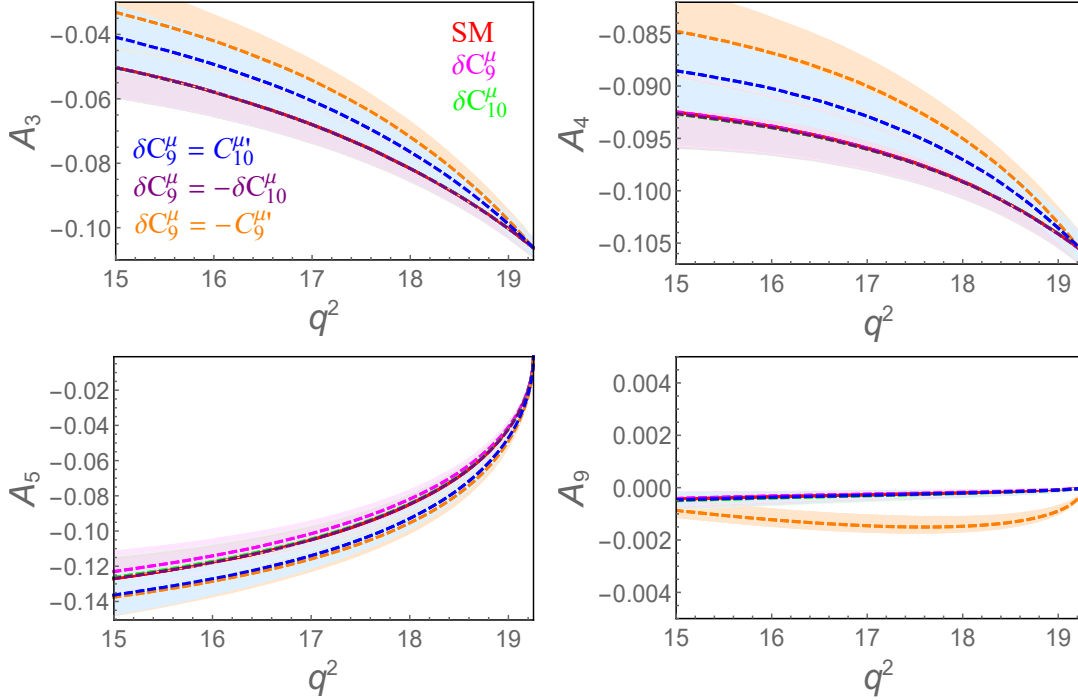


FIG. 2. Dilepton mass squared ( $q^2$ ) spectra of observables  $A_i$  in the SM (solid lines in red) and different NP scenarios (dashed lines). Shaded regions denote the uncertainties of SM and five NP scenarios.

TABLE III. Predictions in the SM and different NP scenarios for binned observables.

Observables	SM	$\delta C_9^\mu$	$\delta C_{10}^\mu$	$\delta C_9^\mu = C_{10}^{\mu'}$	$\delta C_L^\mu$	$\delta C_9^\mu = -C_9^{\mu'}$
$A_3$ [15,19] GeV <sup>2</sup>	$-0.067_{-0.006}^{+0.006}$	$-0.067_{-0.006}^{+0.006}$	$-0.067_{-0.006}^{+0.006}$	$-0.060_{-0.007}^{+0.007}$	$-0.067_{-0.006}^{+0.006}$	$-0.054_{-0.007}^{+0.007}$
$A_4$ [15,19] GeV <sup>2</sup>	$-0.096_{-0.002}^{+0.002}$	$-0.096_{-0.002}^{+0.002}$	$-0.096_{-0.002}^{+0.002}$	$-0.093_{-0.002}^{+0.003}$	$-0.096_{-0.002}^{+0.002}$	$-0.090_{-0.003}^{+0.003}$
$A_5$ [15,19] GeV <sup>2</sup>	$-0.104_{-0.008}^{+0.008}$	$-0.101_{-0.008}^{+0.008}$	$-0.104_{-0.008}^{+0.008}$	$-0.113_{-0.008}^{+0.008}$	$-0.104_{-0.008}^{+0.008}$	$-0.115_{-0.008}^{+0.008}$
$A_9$ [15,19] GeV <sup>2</sup>	$-0.0003_{-0.0002}^{+0.0001}$	$-0.0003_{-0.0002}^{+0.0001}$	$-0.0003_{-0.0002}^{+0.0002}$	$-0.0003_{-0.0002}^{+0.0002}$	$-0.0003_{-0.0002}^{+0.0002}$	$-0.0013_{-0.0002}^{+0.0004}$

By examining Fig. 2 and Table III, we can see that these observables can provide two possible strategies to distinguish between different NP structures. The first strategy is to analyse the  $q^2$  spectra of certain observables. It is clear that the discriminating power of these observables  $A_i(q^2)$  is very limited. For

instance, to distinguish the NP scenario  $\delta C_9^\mu = -C_9^{\mu'}$ , an experimental uncertainty of sub percent level or lower is needed. The second strategy is to study binned observables in proper ranges of  $q^2$ . As shown in Table III, only binned  $A_3$  and  $A_9$  have the ability to discriminate the scenarios  $\delta C_9^\mu = -C_9^{\mu'}$  and  $\delta C_9^\mu = C_{10}^{\mu'}$  at  $3\sigma$  confidence level if they can be measured with an uncertainty of 0.001. However, the rest NP scenarios cannot be discriminated by these observables  $A_i$ .

In conclusion, the angular asymmetries  $A_i$  cannot uniquely distinguish between the five different NP solutions in the one-dimensional scenario.

### B. Sensitivity of ratios $R_i$ to new physics

In this subsection, we study whether the ratios  $R_i$  introduced in Refs. [13, 14] can be used to discriminate the five NP scenarios.

First we plot the  $q^2$  spectra of  $R_i(q^2)$  in a low bin of [1,6] GeV<sup>2</sup> in Fig. 3. One can see that the two observable  $R_{1s}(q^2)$  and  $R_{2s}(q^2)$  could discriminate all the five different NP scenarios, while the observable  $R_{1c}(q^2)$  or  $R_{2c}(q^2)$  can only discriminate the NP scenario  $\delta C_9^\mu = -C_9^{\mu'}$ . As explicitly shown in Appendix B, the other ratios suffer from effects of power corrections and charm loop contributions and have no ability to distinguish the NP scenarios. We stress that it is possible to distinguish the five different NP scenarios if future experimental statistics is high enough such that an uncertainty of percent level or lower can be achieved.

TABLE IV. Same as Table. III but for observables  $R_{1c,1s,2c,2s}$ .

Observables	SM	$\delta C_9^\mu$	$\delta C_{10}^\mu$	$\delta C_9^\mu = C_{10}^{\mu'}$	$\delta C_L^\mu$	$\delta C_9^\mu = -C_9^{\mu'}$
$R_{1s}$ [1,4] GeV <sup>2</sup>	$0.982_{-0.002}^{+0.002}$	$1.13_{-0.02}^{+0.02}$	$0.85_{-0.02}^{+0.03}$	$1.06_{-0.03}^{+0.02}$	$0.95_{-0.03}^{+0.03}$	$1.18_{-0.03}^{+0.02}$
$R_{2s}$ [1,4] GeV <sup>2</sup>	$0.966_{-0.001}^{+0.001}$	$1.11_{-0.02}^{+0.01}$	$0.83_{-0.02}^{+0.02}$	$1.04_{-0.03}^{+0.02}$	$0.93_{-0.02}^{+0.02}$	$1.16_{-0.02}^{+0.02}$
$R_{1c}$ [1,6] GeV <sup>2</sup>	$1.007_{-0.001}^{+0.001}$	$0.84_{-0.01}^{+0.02}$	$0.86_{-0.02}^{+0.02}$	$0.79_{-0.01}^{+0.02}$	$0.82_{-0.01}^{+0.01}$	$0.69_{-0.03}^{+0.05}$
$R_{2c}$ [1,6] GeV <sup>2</sup>	$0.977_{-0.001}^{+0.001}$	$0.81_{-0.01}^{+0.02}$	$0.84_{-0.02}^{+0.02}$	$0.77_{-0.01}^{+0.02}$	$0.79_{-0.01}^{+0.01}$	$0.67_{-0.03}^{+0.05}$

Next, we study binned observables in proper ranges of  $q^2$ . As shown in Table IV, once  $R_{1s}$  or  $R_{2s}$  is measured with the same accuracy as that of theoretical predictions, the five different NP scenarios can be either confirmed or excluded at  $2\sigma$  confidence level. Therefore, the binned observables  $R_{1s}$  and  $R_{2s}$  are useful to distinguish between different NP scenarios, though less constraining than the  $q^2$  spectra.

We therefore conclude that the ratios  $R_{1s}$  and  $R_{2s}$  could uniquely distinguish between the five different NP solutions in the one-dimensional scenario if they can be measured with a precision of percent level.



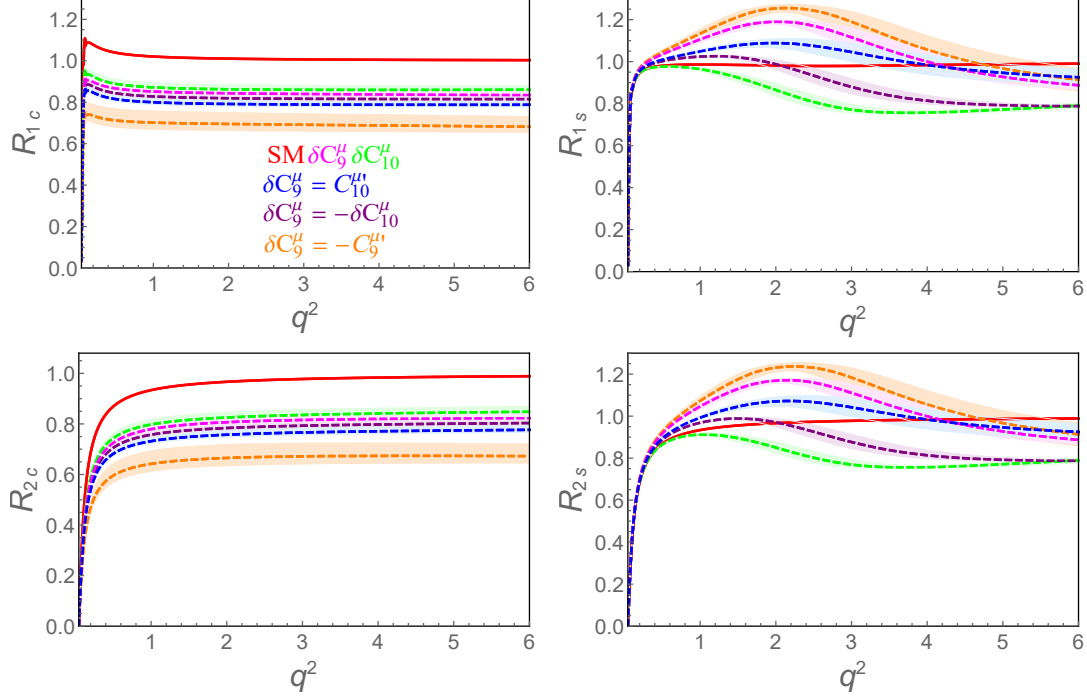


FIG. 3. Same as Fig. 2 but for observables  $R_{1c,1s,2c,2s}$ .

#### IV. SUMMARY AND OUTLOOK

In conclusion, in the one-dimensional NP case only five scenarios, i.e.,  $\delta C_9^\mu$ ,  $\delta C_{10}^\mu$ ,  $\delta C_L^\mu$ ,  $\delta C_9^\mu = C_{10}^{\mu\prime}$  and  $\delta C_9^\mu = -C_9^{\mu\prime}$ , can well describe the latest LHCb, Belle, ATLAS, and CMS data. In order to discriminate the five different NP scenarios, we first “constructed” four angular asymmetries  $A_i$  and study the sensitivity of  $A_i$  to new physics. We find that these observables  $A_i$  cannot discriminate different NP scenarios. Further, we revisited a set of ratios  $R_i$  and showed that the observables  $R_{1s}$  and  $R_{2s}$  can uniquely discriminate the five NP solutions in the one-dimensional case once they are measured in future experiments, by analysing the  $q^2$  spectra of these observables and their binned results.

In the next few years, with the collection of more data at the LHCb, Belle II experiments and improvement of experimental precision, such global fits should be continually updated. In addition, new ideas should be explored to further reduce hadronic uncertainties. Furthermore, it will be interesting to study the interplay between semi-leptonic baryon decays, such as  $\Lambda_b \rightarrow \Lambda$ ,  $\Xi_b \rightarrow \Xi$ , and semi-leptonic meson decays. Because of rich helicity structures, if measured up to the same precision, semi-leptonic baryon decays could constrain more tightly some relevant Wilson coefficients than their mesonic counterparts.

## V. ACKNOWLEDGMENTS

We thank Jorge Martin Camalich for providing the code for the calculation of the  $b \rightarrow s\ell\ell$  amplitudes. This work is partly supported by the National Natural Science Foundation of China under Grants No.11735003, No.11975041, and No.11961141004, and the fundamental Research Funds for the Central Universities.

## VI. APPENDIX

### A. Discussion about NP in the electron and muon channels

In our current work and most works performed so far, NP is assumed to only originate from the muon mode. On the other hand, one can also assume that NP exists in the electron mode, or a combination of the electron and muon modes. In the electron mode, the signs of the fitted Wilson coefficients should be opposite to those of the muon mode if only the observables  $R_K$  and  $R_{K^*}$  are taken into account. The case of allowing for NP in the electron channel has been discussed quite extensively in Refs. [44, 56] (for some recent studies see, e.g., Refs. [37, 40, 57–59]). Here, we investigate a more general scenario that NP comes from a combination of electron and muon channels. As a result, more experimental data need to be taken into account, such as the branching fraction [60] as well as eight angular observables [61, 62] for the  $B \rightarrow K^*e^+e^-$  decay. Thus, the total number of data fitted becomes 103.

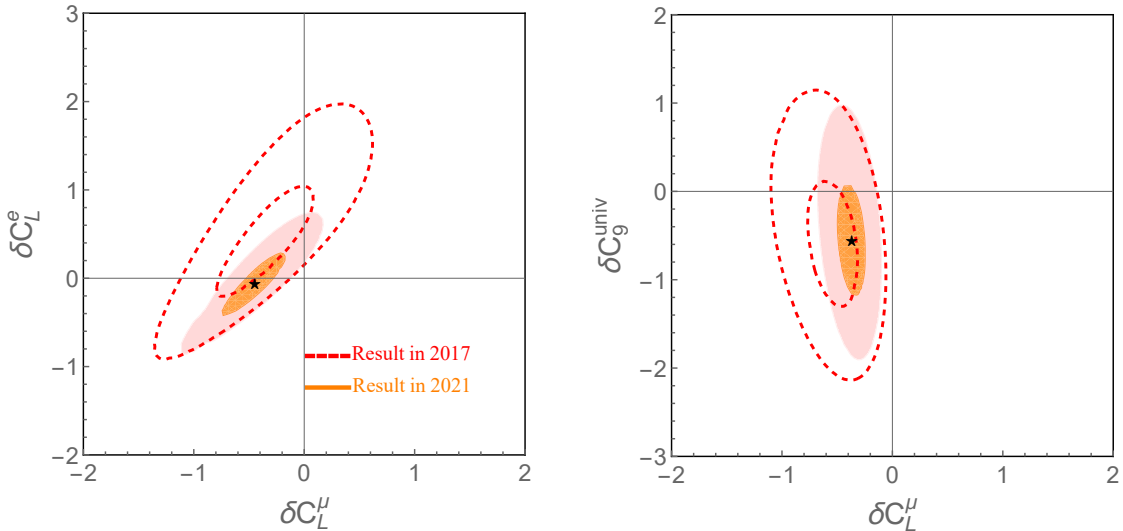


FIG. 4. Contours for the two-parameter fits  $(\delta C_L^\mu, \delta C_L^e)$  and  $(\delta C_L^\mu, \delta C_9^{\text{univ}})$  including the full data set (103 data). The regions in orange and light-red represent the  $1\sigma$  and  $3\sigma$  bounds. The lines in red correspond to those in Fig.7 of Ref. [14].

In Fig. 4, we show the two-parameter fits for the  $(\delta C_L^\mu, \delta C_L^e)$  and  $(\delta C_L^\mu, \delta C_9^{\text{univ}})$  cases including the full 103 data set. Here, one requires  $\delta C_9^{\text{univ}} = \delta C_9^\mu = \delta C_9^e$ . Compared to the results in 2017, all the NP scenarios are better constrained as shown by the smaller contours. In addition, the pure  $\delta C_L^{\text{univ}}$  scenario does not change significantly and is still in agreement with the SM within the  $1\sigma$  confidence level while other scenarios are not. More specifically, the significance of the SM exclusion in the pure  $\delta C_L^\mu$  scenario becomes larger. Also, the new data favor a zero  $\delta C_9^e$  contribution. It should be mentioned that these variations from 2017 to 2021 are mainly caused by the most precise  $R_K$  from the LHCb experiment. The new results indicate that new physics is most likely to exist in the muon mode.

## B. $q^2$ spectra of $R_{3-9}$

In Fig. 5, we show the  $q^2$  spectra of  $R_{3-9}$ . Clearly, these ratios cannot discriminate the five NP scenarios.

- 
- [1] S. L. Glashow, J. Iliopoulos, and L. Maiani, *Phys. Rev. D* **2**, 1285 (1970).
  - [2] Y. Li and C.-D. Lü, *Sci. Bull.* **63**, 267 (2018), arXiv:1808.02990 [hep-ph].
  - [3] S. Bifani, S. Descotes-Genon, A. Romero Vidal, and M.-H. Schune, *J. Phys.* **G46**, 023001 (2019), arXiv:1809.06229 [hep-ex].
  - [4] R. Aaij et al. (LHCb), (2021), arXiv:2103.11769 [hep-ex].
  - [5] R. Aaij et al. (LHCb), *Phys. Rev. Lett.* **113**, 151601 (2014), arXiv:1406.6482 [hep-ex].
  - [6] R. Aaij et al. (LHCb), (2021), arXiv:2108.09283 [hep-ex].
  - [7] R. Aaij et al. (LHCb), (2021), arXiv:2108.09284 [hep-ex].
  - [8] L.-S. Geng, B. Grinstein, S. Jäger, S.-Y. Li, J. Martin Camalich, and R.-X. Shi, *Phys. Rev. D* **104**, 035029 (2021), arXiv:2103.12738 [hep-ph].
  - [9] M. Beneke, C. Bobeth, and R. Szafron, *JHEP* **10**, 232 (2019), arXiv:1908.07011 [hep-ph].
  - [10] A. M. Sirunyan et al. (CMS), *JHEP* **04**, 188 (2020), arXiv:1910.12127 [hep-ex].
  - [11] M. Aaboud et al. (ATLAS), *JHEP* **04**, 098 (2019), arXiv:1812.03017 [hep-ex].
  - [12] S. Jäger and J. Martin Camalich, *JHEP* **05**, 043 (2013), arXiv:1212.2263 [hep-ph].
  - [13] S. Jäger and J. Martin Camalich, *Phys. Rev.* **D93**, 014028 (2016), arXiv:1412.3183 [hep-ph].
  - [14] L.-S. Geng, B. Grinstein, S. Jäger, J. Martin Camalich, X.-L. Ren, and R.-X. Shi, *Phys. Rev.* **D96**, 093006 (2017), arXiv:1704.05446 [hep-ph].
  - [15] R. Aaij et al. (LHCb), *JHEP* **08**, 055 (2017), arXiv:1705.05802 [hep-ex].
  - [16] A. Abdesselam et al. (Belle), (2019), arXiv:1904.02440 [hep-ex].
  - [17] S. Choudhury et al. (BELLE), *JHEP* **03**, 105 (2021), arXiv:1908.01848 [hep-ex].

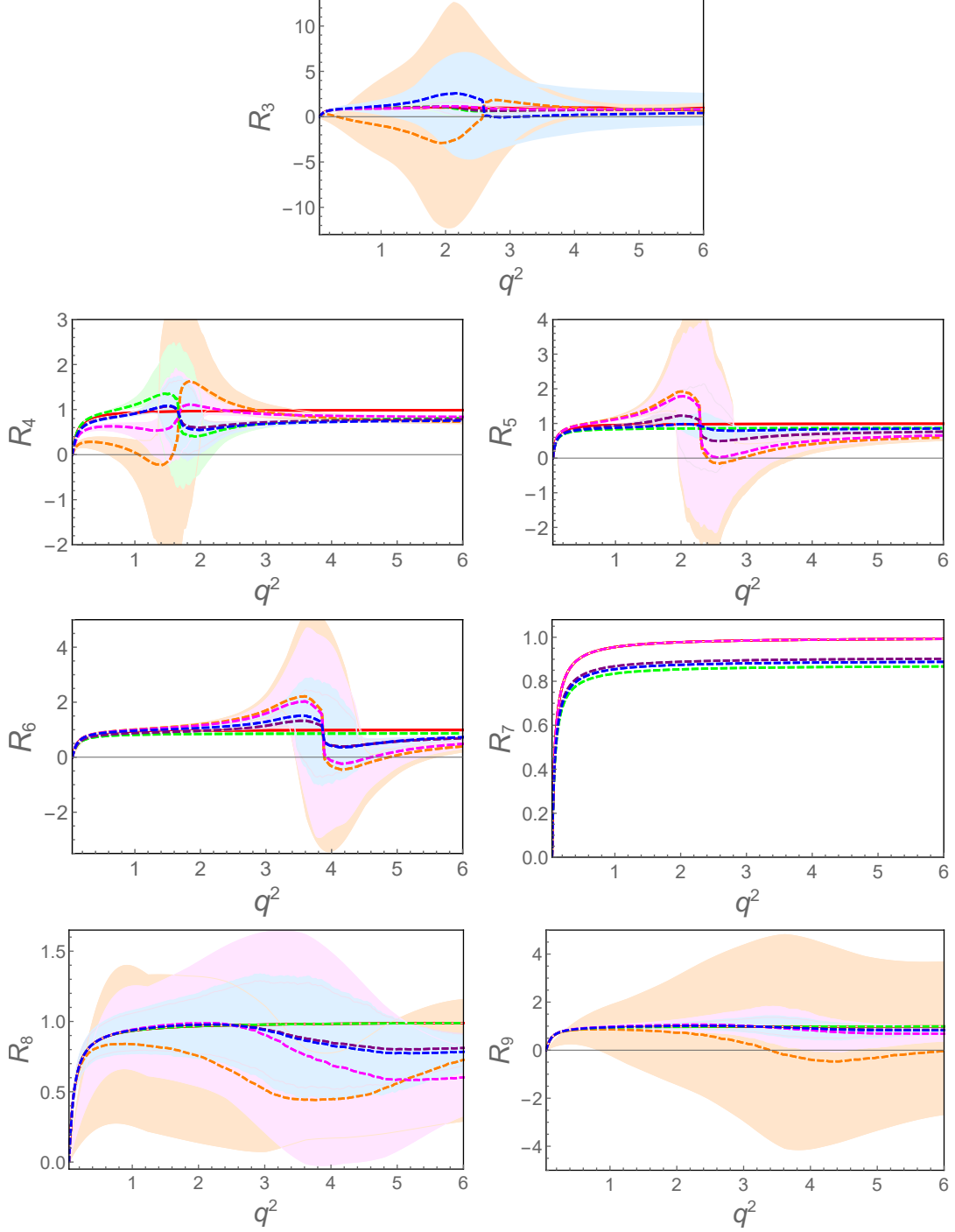


FIG. 5. Same as Fig. 3 but for observables  $R_{3-9}$ .

- [18] R. Aaij et al. (LHCb), Phys. Rev. Lett. **125**, 011802 (2020), arXiv:2003.04831 [hep-ex].
- [19] R. Aaij et al. (LHCb), Phys. Rev. Lett. **126**, 161802 (2021), arXiv:2012.13241 [hep-ex].
- [20] R. Aaij et al. (LHCb), JHEP **02**, 104 (2016), arXiv:1512.04442 [hep-ex].
- [21] W. Altmannshofer and P. Stangl, (2021), arXiv:2103.13370 [hep-ph].

- [22] C. Cornella, D. A. Faroughy, J. Fuentes-Martín, G. Isidori, and M. Neubert, (2021), arXiv:2103.16558 [hep-ph].
- [23] J. Kriewald, C. Hati, J. Orloff, and A. M. Teixeira, in 55th Rencontres de Moriond on Electroweak Interactions and Unified Theories (2021) arXiv:2104.00015 [hep-ph].
- [24] M. Algueró, B. Capdevila, S. Descotes-Genon, J. Matias, and M. Novoa-Brunet, in 55th Rencontres de Moriond on Electroweak Interactions and Unified Theories (2021) arXiv:2104.08921 [hep-ph].
- [25] T. Hurth, F. Mahmoudi, D. M. Santos, and S. Neshatpour, (2021), arXiv:2104.10058 [hep-ph].
- [26] A. Carvunis, F. Dettori, S. Gangal, D. Guadagnoli, and C. Normand, (2021), arXiv:2102.13390 [hep-ph].
- [27] A. Angelescu, D. Bečirević, D. A. Faroughy, F. Jaffredo, and O. Sumensari, (2021), arXiv:2103.12504 [hep-ph].
- [28] D. Lancierini, G. Isidori, P. Owen, and N. Serra, (2021), arXiv:2104.05631 [hep-ph].
- [29] J.-Y. Cen, Y. Cheng, X.-G. He, and J. Sun, (2021), arXiv:2104.05006 [hep-ph].
- [30] J. Kawamura and S. Raby, (2021), arXiv:2104.04461 [hep-ph].
- [31] A. Greljo, P. Stangl, and A. E. Thomsen, (2021), arXiv:2103.13991 [hep-ph].
- [32] T. Nomura and H. Okada, (2021), arXiv:2104.03248 [hep-ph].
- [33] M. Du, J. Liang, Z. Liu, and V. Q. Tran, (2021), arXiv:2104.05685 [hep-ph].
- [34] P. Fileviez Pérez, C. Murgui, and A. D. Plascencia, (2021), arXiv:2104.11229 [hep-ph].
- [35] J. Chen, Q. Wen, F. Xu, and M. Zhang, (2021), arXiv:2104.03699 [hep-ph].
- [36] K. S. Babu, P. S. B. Dev, S. Jana, and A. Thapa, *JHEP* **03**, 179 (2021), arXiv:2009.01771 [hep-ph].
- [37] A. K. Alok, A. Dighe, S. Gangal, and D. Kumar, *JHEP* **06**, 089 (2019), arXiv:1903.09617 [hep-ph].
- [38] F. Munir Bhutta, Z.-R. Huang, C.-D. Lü, M. A. Paracha, and W. Wang, (2020), arXiv:2009.03588 [hep-ph].
- [39] A. K. Alok, S. Kumbhakar, J. Saini, and S. U. Sankar, *Nucl. Phys. B* **967**, 115419 (2021), arXiv:2011.14668 [hep-ph].
- [40] J. Kumar and D. London, *Phys. Rev.* **D99**, 073008 (2019), arXiv:1901.04516 [hep-ph].
- [41] A. K. Alok, B. Bhattacharya, D. Kumar, J. Kumar, D. London, and S. U. Sankar, *Phys. Rev. D* **96**, 015034 (2017), arXiv:1703.09247 [hep-ph].
- [42] B. Capdevila, A. Crivellin, S. Descotes-Genon, J. Matias, and J. Virto, *JHEP* **01**, 093 (2018), arXiv:1704.05340 [hep-ph].
- [43] M. Algueró, P. A. Cartelle, A. M. Marshall, P. Masjuan, J. Matias, M. A. McCann, M. Patel, K. A. Petridis, and M. Smith, (2021), arXiv:2107.05301 [hep-ph].
- [44] T. Hurth, F. Mahmoudi, D. Martinez Santos, and S. Neshatpour, *Phys. Rev.* **D96**, 095034 (2017), arXiv:1705.06274 [hep-ph].
- [45] B. Capdevila, S. Descotes-Genon, J. Matias, and J. Virto, *JHEP* **10**, 075 (2016), arXiv:1605.03156 [hep-ph].
- [46] W. Altmannshofer, P. Stangl, and D. M. Straub, *Phys. Rev. D* **96**, 055008 (2017), arXiv:1704.05435 [hep-ph].
- [47] S. Descotes-Genon, J. Matias, and J. Virto, *Phys. Rev. D* **88**, 074002 (2013), arXiv:1307.5683 [hep-ph].
- [48] S. Descotes-Genon, L. Hofer, J. Matias, and J. Virto, *JHEP* **06**, 092 (2016), arXiv:1510.04239 [hep-ph].

- [49] W. Altmannshofer, P. Ball, A. Bharucha, A. J. Buras, D. M. Straub, and M. Wick, *JHEP* **01**, 019 (2009), arXiv:0811.1214 [hep-ph].
- [50] R. Mandal, R. Sinha, and D. Das, *Phys. Rev.* **D90**, 096006 (2014), arXiv:1409.3088 [hep-ph].
- [51] A. K. Alok, S. Kumbhakar, and S. Uma Sankar, (2020), arXiv:2001.04395 [hep-ph].
- [52] T. Hurth, F. Mahmoudi, and S. Neshatpour, *Nucl. Phys.* **B909**, 737 (2016), arXiv:1603.00865 [hep-ph].
- [53] S. Bhattacharya, A. Biswas, S. Nandi, and S. K. Patra, *Phys. Rev.* **D101**, 055025 (2020), arXiv:1908.04835 [hep-ph].
- [54] M. Santimaria, in LHCb Seminar at CERN (March 23th 2021).
- [55] W. Altmannshofer, S. Gori, M. Pospelov, and I. Yavin, *Phys. Rev. D* **89**, 095033 (2014), arXiv:1403.1269 [hep-ph].
- [56] M. Ciuchini, A. M. Coutinho, M. Fedele, E. Franco, A. Paul, L. Silvestrini, and M. Valli, *Eur. Phys. J.* **C77**, 688 (2017), arXiv:1704.05447 [hep-ph].
- [57] M. Ciuchini, A. M. Coutinho, M. Fedele, E. Franco, A. Paul, L. Silvestrini, and M. Valli, *Eur. Phys. J.* **C79**, 719 (2019), arXiv:1903.09632 [hep-ph].
- [58] M. Algueró, B. Capdevila, S. Descotes-Genon, P. Masjuan, and J. Matias, *Phys. Rev.* **D99**, 075017 (2019), arXiv:1809.08447 [hep-ph].
- [59] M. Algueró, B. Capdevila, S. Descotes-Genon, P. Masjuan, and J. Matias, *JHEP* **07**, 096 (2019), arXiv:1902.04900 [hep-ph].
- [60] R. Aaij et al. (LHCb), *JHEP* **05**, 159 (2013), arXiv:1304.3035 [hep-ex].
- [61] R. Aaij et al. (LHCb), *JHEP* **04**, 064 (2015), arXiv:1501.03038 [hep-ex].
- [62] R. Aaij et al. (LHCb), *JHEP* **12**, 081 (2020), arXiv:2010.06011 [hep-ex].